Resilin, the gene for the molecular spring: its roles in flight and jumping of *Drosophila*

Miyuna Hagiwara[1], Yoshiki Eto[2], Yoko Keira[2], Hiroyuki O. Ishikawa[2], Takaomi Sakai[1], Toshiro Aigaki[1], Tsunaki Asano[1,*]

[1] Department of Biological Sciences, Tokyo Metropolitan University
[2] Department of Biology, Chiba University

*Corresponding Author: asano-tsunaki@tmu.ac.jp, Minami Osawa 1-1, Hachioji city, Tokyo, Japan
Email: asano-tsunaki@tmu.ac.jp
Tell: +81-426-771-111
Fax: +81-426-772-559

Abstract

Resilin is a member of the chitin-binding protein family that was originally found as a major component of an elastic matrix present in insects. The knockdown of the gene for this protein in *Drosophila melanogaster* causes the characteristic downturned wing posture, and the knockdown flies cannot move their wings. The jump distance of the knockdown flies is around 50% shorter than that of the controls. Null mutant flies show the same phenotypes, which can be rescued by introducing a 4.7 kb genomic fragment harboring the whole coding region of *Resilin*. *In vitro* experiments have shown that the elasticity of the matrix made of Resilin is due to the dityrosine-mediated polymerization of Resilin molecules. Dual oxidase (Duox) is the most likely candidate for the *in vivo* polymerization of Resilin molecules. *Duox* knockdown induces phenotypes similar to those observed in wing posture and jump performance of the *Resilin* knockdown and knockout flies, which can be rescued by the overexpression of *Duox* gene from a beetle. These findings suggest that Duox is an essential factor for the proper function of Resilin as the major component of the resilin matrix.

Introduction

Insects are often regarded as the most successful animals on Earth with their extreme diversity, enormous biomass, and great impact on the global ecosystem. There have been intensive debates as to why insects have been so successful, and their ability to fly must have had great impacts on their evolutionary process and the expansion of their habitat to a wide range of terrestrial environments. It is considered that the ability to fly is advantageous in the competition for survival and the creation of new niches not easily accessible to other animals, which is supported by the fact that 99% of the described insect species are winged.

During powered flight, insects flap their wings by moving their flight muscles in the thorax. Repetitive and rapid contractions of flight muscles are transformed into high-frequency wing motion, generating a force to lift the insect's body[1,2]. The hinges connecting the wings and the body have thick tendons, which may be involved in energy transformation from the flight muscles to the wings[3,4]. Accumulation of mechanical loads derived from the high-frequency vibration during flight could eventually destroy structures around the wing hinges. However, the thick tendon of the

wing hinges is composed of a rubber-like matrix, which may presumably absorb/relieve such stresses, and prevent the hinges from breaking down[3,4,5]. In addition to their powered flight, insects may also use the properties of such rubber-like matrices for jumping. Similarly to flight, jumping is a high-velocity locomotion through the air, which may be another advantage of insects that is not found in other invertebrates, with only a few exceptions of some arthropods, such as sand hoppers or jumping spiders[6,7,8]. It has been reported that the rubber-like matrices are found in the joints of the hind legs of the locust or in the pleural arch at the top of the hind legs of the flea. Both of which are positioned in places that can be easily imagined to be used as a spring providing highly efficient energy kinetics for achieving long-distance and high-velocity locomotion[7,9,10].

The first description of the rubber-like matrices in insects was the discovery of tendons in the wing hinges of dragonflies and locusts[4]. At that time, the rubber-like matrices were named “resilin” after the Latin word “resilire,” which means resilience, and were defined as materials that can be stained with methylene blue or toluidine blue. After that, rubber-like matrices (hereafter, referred to as the “resilin matrix”) were

65 found in the salivary pump and feeding pump of bags, or the tymbal of cicadas for

66 sound production[11,12]. The connection between jumping mechanisms and the

67 localization of the resilin matrix at leg joints has also been discussed in insects such as

68 locusts that have the thick resilin matrix at the joints of their hind legs[9,13]. Relatively

69 recent reports on the functions of the resilin matrix include examples from bed bugs

70 and midges. Male common bedbugs (*Cimex lectularius* and *Cimex hemipterus*)

71 puncture the intersegmental membrane of the female abdomen with a needle to inject

72 their sperm. After the male detaches from the female, the pore is likely closed,

73 probably owing to the elasticity of the resilin matrix[14,15]. Larvae of the phantom midge

74 (*Chaoborus americanus*) can regulate their buoyancy by altering the volume of their

75 air sacs. This is achieved through a pH-dependent transition in the shape of the resilin

76 matrix that composes the air sacs. During this process, membrane ATPase controls the

77 proton content of the resilin matrix[16].

78 The physical properties of the resilin matrix are not affected considerably by

79 deep freezing, high temperature, or treatments with alcohols or fixatives. In contrast,

80 the resilin matrix is rapidly dissolved by proteolytic digestion, indicating that proteins

81 are its major constituents[4]. Subsequently, a study showed that proteins in the resilin

82 matrix are crosslinked together through the formation of di- or tri-tyrosine, in which

83 tyrosine residues are covalently crosslinked to each other[17]. It was also shown that di-

84 and tri-tyrosine emit the characteristic blue fluorescence under UV irradiation, and this

85 property has been used as a useful tool to observe the localization of the resilin matrix

86 noninvasively (hereafter, di- and tri-tyrosine are collectively referred to as dityrosine).

87 In 2001, Ardell and Andersen reported a candidate gene encoding a protein composing

88 the resilin matrix. Partial amino acid sequences of peptides isolated from the protease

89 digest of the resilin matrix taken from the desert locust *Schistocerca gregaria* were

90 determined by Edman degradation. The obtained sequences were used for BLAST

91 search in the genomic database of the fruit fly *Drosophila melanogaster* to find

92 candidate genes encoding *Drosophila* proteins homologous to the locust proteins[18].

93 Two proteins (CG15920 and CG9036) were found to have the sequences that matched

94 well with those obtained from the resilin matrix of the locust. On the basis of similarity

95 in amino acid compositions (high amounts of proline, glycine, and tyrosine), Ardell &

96 Andersen concluded that CG15920 was the most likely candidate, and tentatively

97 named the *CG15920 "Resilin*" as the gene for a major protein composing the resilin

98 matrix. Since that study, *CG15920* has been called *Resilin* (hereafter, *Rsl*). Until

99 recently, however, there had been no reports on the gene function analysis to directly

100 demonstrate that the gene encoding resilin is actually involved in insect flight or

101 jumping. Furthermore, it was also not known how resilin molecules are polymerized *in*

102 *vivo*, although *in vitro* experiments using a recombinant Rsl protein of *D. melanogaster*

103 have shown that Rsl polymerization is necessary for the high elasticity of synthetic

104 resilin matrix[5,19-21].

105 Here, using the newly obtained *Rsl* mutant of *D. melanogaster*, we characterized

106 the phenotypes and showed that *Rsl* has roles in preventing the breakdown of the wing

107 hinge structure over time and in efficient jumping. We also tried to show which genes

108 were involved in the polymerization of the Rsl molecule. Dual oxidase (Duox) is a

109 membrane protein with the extracellular peroxidase domain and the transmembrane

110 NADPH-oxidase domain. By tissue-specific *Duox* knockdown and its rescue

111 experiment, we showed that Duox was indeed the factor for Rsl polymerization. We

112 also showed that the Duox-mediated polymerization of Rsl was indispensable for the

113 proper function of the Rsl/resilin matrix both in flight and jumping, which may be the

114 critical factors for the evolution and success of insects as terrestrial organisms.

115 **Results**

116 ***Rsl* encodes a protein with "elastic repeats"**

117 *Rsl* is composed of three exons, and two isoforms *Rsl-RA* and *Rsl-RB* (with and

118 without exon 2, respectively) are expressed (Figure 1A)[22,23]. Rsl is the secreted protein

119 with a signal sequence (Figure 1B)[18]. The polypeptide encoded by *Rsl-RA* is divided

120 into three parts: 1) repeats of N-terminally located "elastic modulus", 2) chitin-binding

121 motif, and 3) repeats of C-terminally located "elastic modulus". The polypeptide

122 encoded by *Rsl-RB* is devoid of the large portion of the chitin-binding motif (Figure

123 1B)[18,24].

124 The elastic moduli[24] (hereinafter referred to as elastic repeats) that are indicated

125 by light-blue or light-green boxes (Figure 1B) are characterized by the consensus

126 sequences containing proline, glycine, and tyrosine. The consensus sequences are also

127 found in other insect proteins that are annotated as resilin[23,24]. The tyrosine residue is

128 considered important for the formation of intermolecular crosslinks[18]. As first

129 described by Ardell and Andersen[18], the consensus sequences of the elastic repeats in

130 the N- and C-terminal regions are different from each other (Figure 1B). In *D.*

131 *melanogaster*, the N-terminal repeats (-**P**--<u>Y</u>G-**P**G---) have two prolines with an

132 intervening tyrosine, whereas the C-terminal repeats (G<u>Y</u>S-GR**P**GG) have only one

133 tyrosine and one proline. In the multiple sequence alignment[23,24], the N-terminal

134 repeats are conserved among species, but there are at least two subtypes in the

135 consensus sequences of the C-terminal repeats. In many insects, the consensus is

136 G<u>Y</u>**P**SGG**P**GG with two prolines (type-A repeat). In contrast, many fly species and a

137 portion of hemipteran insects have different consensus sequences characterized by the

138 presence of only one proline (Figure 1B). In a comprehensive database search of

139 arthropod genomes, we found that in amino acid sequences of resilins from the

140 palaeopteran insects (Odonata and Ephemeroptera: the orders of the most primitive

141 winged insects) or those from the collembolan (the primitive non-insect hexapods), no

142 consensus sequences of the C-terminal repeats are found (Figure S1). Considering the

143 branching pattern of the phylogenetic tree illustrating the evolutionary process of

144 insects (see Figure S1), it can be hypothesized that the C-terminal repeats are a trait

145 that was obtained in accordance with the emergence of a new type of winged insects

146 (Neoptera). In the three-dimensional model of *Drosophila* Rsl (Q9V7U0 in the uniplot

147 database), which was predicted using AlphaFold Server (https://alphafoldserver.com)

148 powered by AlphaFold 3[25] (Figure 1C), both the N- and C-terminal regions have a

149 spring-like "coiled" shape (panels b and c, respectively), with each elastic repeat

150 corresponding to one cycle of the spring (panels d and e). The presence of the beta turn

151 at the short PGG sequence motif in the C-terminal repeats (arrowheads in panel c) is

152 consistent with the previous prediction[18]. Our predictions using AlphaFold 3 showed a

153 spring-like shape similar to the Rsl model in the resilin of other insects, except for

154 species such as *Bombyx mori* (Lepidoptera) and *Folsomia candida* (Collembola)

155 (Figure S2). The spring-like "coiled" shape in the models is intriguing, considering the

156 function of the resilin as a component of spring-rubber-like biomaterials.

157

158 ***Rsl* is expressed in the wing hinge and the leg joint**

159 In previous studies of the two Drosophilidae species[22,26], it was shown that *Rsl* was

160 mainly expressed in late pupal stages. In our RT-PCR analysis (Figure 2A), the

161 apparent signals of the isoforms *Rsl-RA* and *Rsl-RB* were detected from the pupal to

162 early adult stages. From 2 to 4 days after puparium formation (APF), the signals for

163 *Rsl* expressions are strong, and the emergence of the signal for the expression of

164 *Rsl-RB* precedes that of *Rsl-RA*. In western blotting with the specific antibody, two

165 signals corresponding to the molecular masses of 57k and 52k can be seen (Figure 2B).

166 The upper and lower signals correspond to mature Rsl-PA and Rsl-PB without a signal

167 sequence, respectively (Figure S3). The emergence of the Rsl-PB signal precedes that

168 of Rsl-PA, which is consistent with the temporal patterns obtained by RT-PCR analysis

169 (Figure 2A). Rsl signals almost disappear after eclosion, which is consistent with the

170 observation that resilin molecules are polymerized to become insoluble materials[17]. Rsl

171 polymer cannot penetrate into the SDS-PAGE gel and are not detectable by western

172 blot analyses.

173 To see the spatial patterns of *Rsl* expression, we prepared the *Rsl* promoter-Gal4

174 driver that covers the genomic region around 2.3 kbp upstream of the first ATG (Figure

175 1A). The expression was visualized using the *UAS-Rsl-RA*::*mCherry* reporter. The

176 photos in Figure 2C show pupae on day 3 APF. The mCherry signal was visible at the

177 hinges of the wings, spiracles, compound eyes, and labrum (Figure 2C, panels a, b, and

178 c). In the observation of the adult on day 3 after eclosion, the mCherry signal can be

179 seen on the ventral side of the leg joints between the trochanter and the femur, and the

180 roots of the mechanosensory hairs of the leg and wing (Figures 2D and 2E). These

181 expression patterns were obtained using flies carrying the *Rsl*-promoter Gal4 sequence

182 integrated into the 3rd chromosome. The mCherry signal pattern obtained with the

183 *Rsl*-promoter Gal4 sequence on the second chromosome was nearly identical to the

184 data obtained with *Rsl*-promoter Gal4 on the third chromosome, except that the signal

185 in the compound eyes was very weak (Figure S4). In western blot analysis of the

186 compound eye (Figure 2F), the signals of Rsl can be seen in the wild-type fly, and this

187 signal disappeared in the sample from Rsl^{KO} that we generated (Figures 1A and S5).

188 The results of the western blot analysis indicate that the signal in the wild-type fly

189 corresponds to Rsl, and that the compound eye surely expresses *Rsl*.

190 To observe the details of the internal structure at the wing hinge, we removed the

191 outer cuticle. The mCherry signal was clearly visible just beneath the wing hinge

192 (Figure 2G, panel i), and the structure exhibited blue fluorescence under UV irradiation

193 (Figure 2H). The intensity of this blue fluorescence signal decreased markedly and

194 increased under acidic and alkaline conditions, respectively (see Figure S6), consistent

195 with the characteristics of dityrosine previously reported[17]. This structure, which is

196 positive for both the mCherry signal and blue fluorescence, is the tergopleural tendon.

197 Previous studies have shown that this tendon is the structure connecting the direct

198 flight muscle and the root of the wing at the wing hinge[27-29].

199 Since Rsl-PA has the chitin-binding domain (Figure 1B), we consider that this

200 domain may function in chitin binding. To visualize the distribution of the chitin fiber

201 inside the tergopleural tendon, we expressed ChtVis-tdTomato with *Rsl*-promoter-Gal4.

202 A strong signal can be seen along the horizontal midline, indicating the presence of

203 chitin along the midline (Figure 2I). This is similar to the spatial pattern of

204 Rsl-RA::mCherry (Figure 2H). Next, we compared the distributions of

205 Rsl-RA::mCherry and Rsl-RB::mCherry (with and without the sequence of the

206 chitin-binding domain, respectively) that were separately expressed (Figure 2J). The

207 spatial pattern of Rsl-RA::mCherry, which is denser along the horizontal central line

208 (panel p), contrasts with the more uniform distribution of Rsl-RB::mCherry (panel q).

209 In the calculation for the biased distribution of mCherry signals (see Materials and

210 Methods), the value was higher in flies expressing Rsl-RA::mCherry than in those

211 expressing Rsl-RB::mCherry. This indicates a more uniform distribution of

212 Rsl-RB::mCherry, which may be caused by the absence of a chitin-binding domain.

213

214 ***Rsl* may work to prevent the breakdown of a tendon in the wing hinge that is**

215 **required for sustainable flight**

216 To examine the effects of the suppression of *Rsl* expression, we knocked down Rsl^{30}

217 with the *Rsl*-promoter Gal4 driver, and the expression was suppressed to around the

218 baseline levels (Figure S7). In the *Rsl* knockdown flies, no visible phenotypes were

219 observed in the very early stages of the adult, but after one day, all the knockdown

220 individuals were unable to move their wings and started to display the characteristic

221 downturned wing posture (Figure 3A). The same wing posture has been observed in

222 multiple studies including the analysis of *pink1*, which functions in muscle

223 development[31,32]. The phenotypes observed in our *Rsl* knockdown are the same as

224 those previously reported for the *Rsl* knockdown flies[21]. To further characterize the

225 function of *Rsl*, we used the null mutant (Rsl^{KO}) that was prepared in this study (Figure

226 S5). The homozygous Rsl^{KO} flies showed the characteristic downturned wing posture,

227 and they could not move their wings, which are the same phenotypes as those observed

228 in *Rsl* knockdown flies (Figure 3C, see Extended data Video 2). To rescue these

229 phenotypes, we generated flies with the transgene of the 4.7 kbp genomic fragment

230 harboring the *Rsl* coding region on the 3rd chromosome (*Rsl*-Genomic rescue: *Rsl-GR*)

231 (Figure 1A). The Rsl^{KO} flies with *Rsl-GR* did not show the downturned wing posture

232 (Figures 3C and 3D), and they could move their wings and fly (see Supplementary

233 mov. S3), indicating that *Rsl-GR* rescued the phenotypes of Rsl^{KO}. Then, we also tried

234 to rescue the phenotypes of Rsl^{KO} using the Gal4/UAS system (Figure 3D). Although

235 flies expressing each isoform only gradually showed the wing posture phenotype, the

236 phenotype was almost rescued. Combining the two isoforms did not show markedly

237 different results with those obtained from either *Rsl-RA* or *Rsl-RB* alone.

238 It was shown in *D. melanogaster* that the tergopleural tendon was stained with

239 the anti-Rsl antibody[28], which is consistent with the presence of the signal for the

240 Rsl::mCherry reporter at the tergopleural tendon (Figures 2G and 2H). In Figure 3E,

241 the structure around the tergopleural tendon of the wild-type fly was illustrated

242 according to the previous descriptions [28,29]. The proximal side of the tergopleural

243 tendon is attached to the inner side of the cuticle located at the wing hinge (indicated

244 by the yellow arrowhead), and the direct flight muscles (tergopleural muscles 1 and 2:

245 TP-1 and TP-2, respectively) are attached to both the tergopleural tendon and the

246 cuticle of the body wall. In observation of the inner structure of wing hinges,

247 *dumpy-YFP* (*dpy-YFP*) was used to visualize the boundary between the tendon and the

248 muscle (Figure 3F, panel a). The green signal of Dpy-YFP surrounds the tergopleural

249 tendon emitting the blue fluorescence upon UV irradiation (Figure 3F, panel a). Like

250 the schematic figure (Figure 3E), the direct flight muscles are attached to the

251 tergopleural tendon that is visualized with Dpy-YFP. As shown in panel b of Figure 3F,

252 in the newly emerged Rsl^{KO} fly, no blue fluorescence signal of dityrosine was seen.

253 The loss of dityrosine signals can be explained by the absence of Rsl, which is

254 supposed to provide the tyrosine residues as the source of dityrosine. The tergopleural

255 tendon of the newly emerged Rsl^{KO} fly remained linked to the root of the wing (white

256 arrowheads), which may correlate with the absence of wing posture or movement

257 abnormalities (Figure 3D). In contrast, in Rsl^{KO} flies exhibiting the downturned wing

258 posture (panel c), the tergopleural tendon was ruptured into two pieces (white

259 arrowheads), confirming that the connection between the muscle and the root of the

260 wing was almost lost. In contrast, in *Rsl*^{KO} flies with *Rsl-GR* (panel d), the blue

261 fluorescence that is surrounded by the Dpy-YFP signal is clearly visible. The structures

262 of TP-1 and TP-2 are the same as those observed in wild-type flies, and no damage

263 was observed. This is consistent with the *Rsl*^{KO} flies with *Rsl-GR* showing no

264 phenotypes of wing posture and movement abnormalities (Figures 3C and 3D;

265 Extended data Video 3).

266 In the fields of anatomy and biomechanics, many reports define "resilin" as an

267 extracellular structure that exhibits blue fluorescence, which is characteristic of

268 dityrosine[33]. The blue fluorescence signal has been found in various body parts,

269 including the intersegmental membrane, compound eyes, and wings[34,35]. In this study,

270 to characterize the nature of the blue fluorescence in detail, we focused on the wings,

271 since the presence of the blue fluorescence signal in wings has been reported in

272 multiple insect species[34,35]. In the fly with *Rsl-RA::mCherry* expression that was driven

273 by *Rsl-Gal4*, (Figure S8, panels, a and b), strong mCherry signal can be seen in several

274 places including the tergopleural tendon. In contrast, there is almost no signal at the

275 wing, although with UV, blue fluorescence can be seen at the proximal part of the

276 wings (panel c). This finding suggests that *Rsl* is not expressed even in the area

277 positive for blue fluorescence. In the magnified photo of the wild type fly's wing

278 (Figure S8, panel e), the arrows indicate distinct blue fluorescence signals at the

279 proximal part of the wing, roughly corresponding to the area with landmarks adopted

280 in a previous study (panel d)[36]. These signals became weaker drastically under acidic

281 conditions (panel f), suggesting that they corresponded to dityrosine. In the wing of the

282 Rsl^{KO} fly (panel g), however, the signals were still seen, indicating that not Rsl but

283 other tyrosine-rich substances are the cause of the blue fluorescence signal. These

284 findings support the idea that dityrosine-rich structures exist without *Rsl* in *D.*

285 *melanogaster*.

286

287 **Rsl is polymerized by the enzyme for ROS production**

288 It has been shown that Duox is involved in dityrosine formation in ecdysozoans such

289 as nematodes and insects[37-39]. The ROSs produced in the peroxidase domain may

290 oxidize a tyrosine residue to form a tyrosine phenoxyl radical, followed by the reaction

291 with the neighboring tyrosine residue to produce dityrosine or trityrosine[37,38]. Duox

292 may be the most plausible candidate factor responsible for Rsl polymerization, because

293 Rsl molecules are polymerized through dityrosine formation[17]. To demonstrate this, we

294 examined the effect of *Duox* knockdown on Rsl polymerization or other phenotypic

295 characteristics. In this study, we performed tissue-specific *Duox* knockdown with

296 *Rsl-Gal4*, because whole body knockdown or knockout of *Duox* leads to lethality[37,40].

297 We used two UAS-lines, NIG stock #3131R-3 (*NIG3131R-3*) and the previously

298 reported *UAS-Duox-RNAi*$_{976\text{-}1145}$[40], for *Duox* knockdown. In both cases, immediately

299 after eclosion, *Duox* knockdown flies were able to fold and move their wings normally,

300 but within a day, all of them exhibited the downturned wing posture, similar to *Rsl*

301 knockdown and knockout (Figures 4A and 4B). After emergence of this wing posture,

302 both the *Duox* knockdown flies could not move their wings, similarly to *Rsl*

303 knockdown and knockout flies (hereafter, we mainly performed phenotypic

304 characterization using *NIG3131R-3*).

305 To examine the cause of the downturned wing posture in *Duox* knockdown flies,

306 we performed western blot analysis to determine whether Rsl molecules were

307 polymerized. As shown in Figure 4C, in the *Duox* knockdown flies, the signal for Rsl

308 can be seen at the same electrophoretic mobility of Rsl monomers (Figure 4C, right

309 panel), suggesting that a portion of Rsl molecules remained unpolymerized. This is in

310 contrast to the patterns of the control (Figure 4C, left panel) and wild-type flies (Figure

311 2B), in which the Rsl signals disappeared after eclosion. Another explanation for the

312 detection of *Rsl* in the *Duox* knockdown flies could be the enhancement of *Rsl*

313 expression after becoming adults. However, there were no marked differences in the

314 patterns of *Rsl* expression between the control and the *Duox* knockdown flies (Figure

315 S9), which does not negate the model of the Duox-mediated Rsl polymerization

316 (Figure 4D).

317 We also observed the structure around the tergopleural tendon of the *Duox*

318 knockdown flies (Figure 4E). In the control flies (panels a and b), the structures were

319 almost the same as those of the wild type (Figure 3F), as can be judged from the

320 presence of the blue fluorescence signal at the tergopleural tendon. In the *Duox*

321 knockdown flies, the signal for dityrosine in the tergopleural tendon (indicated by the

322 dotted line in panel c) was very weak. In the *Duox* knockdown flies, the TP-1 and TP-2

323 were completely detached from the tergopleural tendon with the signal of Dpy (panel

324 d), as illustrated in panel e.

325 To rescue the phenotypes caused by *Duox* knockdown, we prepared a UAS-line

326 for expressing of *T. castaneum Duox* (*TcDuox*) as a transgene with a base sequence that

327 is not similar to that of *D. melanogaster Duox*. As shown in Figure 4F, *Duox*

328 knockdown flies with additional *TcDuox* expression did not exhibit the downturned

329 wing posture, even one week after eclosion (Figures 4F and 4G). The flies could move

330 their wings normally and fly (our observation). In western blot analysis, the Rsl signal

331 disappeared within two days after eclosion (Figure 4H, right panel), in contrast to the

332 control flies in which the Rsl signal remained detectable even after two days (left

333 panel). The anatomical structure around the tergopleural tendon was almost the same

334 as that of the wild type (Figure 4I, right panel), which can be judged from the presence

335 of the blue fluorescence signal in the tergopleural tendon, and also the connection

336 between the tergopleural tendon and TP muscles. These findings indicate that the

337 expression of *TcDuox* rescued the phenotypes of the *Duox* knockdown flies, and that

338 *Duox* is the actual factor responsible for Rsl polymerization and the proper functioning

339 of Rsl/resilin matrix in the maintenance of the structure around the wing hinges. We

340 then examined biochemically the Duox-mediated Rsl polymerization through

341 dityrosine formation. Here, commercially available peroxidase was used as the catalyst,

342 instead of the peroxidase domain of Duox, because we were unable to synthesize the

343 functional peroxidase domain of Duox successfully. In the western blot analysis of the

344 truncated version of the recombinant Rsl (reRsl), which was synthesized in an *E. coli*

345 system, reRsl migrated at an electrophoretic mobility corresponding to the predicted

346 molecular mass of 35 k (Figure 4J, left panel, lane a). After treatment with either

347 peroxidase or hydrogen peroxide (lanes b and c), reRsl can be seen at its original

348 mobility. In contrast, in the presence of both peroxidase and hydrogen peroxide, the

349 reRsl signal was shifted to an electrophoretic mobility corresponding to a much higher

350 molecular mass (lane d). As indicated by closed arrowheads, the strong smear signal

351 was seen from the entry site of the concentration gel. The shift of the Rsl signal to an

352 electrophoretic mobility corresponding to high-molecular masses indicates that the Rsl

353 molecules formed a high-molecular mass complex. In the western blot analysis with

354 the antibody against dityrosine (right panel), signals are visible only in the sample

355 treated with both peroxidase and hydrogen peroxide (lane h). The signal is strongest at

356 the entry site of the concentration gel (closed arrowhead), indicating the presence of

357 reRsl, which is highly polymerized by the formation of a large number of dityrosines.

358

359 **Both the expressions of *Rsl* and *Duox* are required for high jump performance**

360 It has been proposed that the resilin matrix may enable high performance in jumping in

361 several insects, such as the flea and locust[10, 21,41,42]. In this study, as a method to

362 quantify the jump performance in *D. melanogaster*, we measured the jump distance

363 using de-winged flies (Figure 5A). In the control flies, their jump distance was around

364 2 cm, but in the *Rsl* knockdown flies, their jump distance was shorter by around half of

365 that of the control (Figure 5B). Also, in Rsl^{KO} flies, the jump distance was almost half

366 of that of the wild-type flies (Figure 5C, Extended data Video 4 and 5). The jump

367 distance of the Rsl^{KO} flies with *Rsl-GR* was almost the same as that of the wild-type

368 flies (Figure 5C), indicating that the phenotype of shorter jump distance was rescued

369 by *Rsl-GR*. In the rescue experiment using the Gal4/UAS system, we were unable to

370 obtain data clearly showing the successful rescue with either *UAS-Rsl-RA* or

371 *UAS-Rsl-RB*. Therefore, presently, we do not have information on the functional

372 differences in jumping between Rsl-PA and Rsl-PB (not shown).

373 Here, in addition to *Rsl*, we examined the contribution of *Duox* to fly jumping.

374 *Duox* was knocked down with either of *NIG3131R-3* or *UAS-Duox-RNAi*$_{976\text{-}1145}$, and in

375 both cases, the jump distances of the knockdown flies were around half of that of the

376 controls (Figure 5D). To rescue this phenotype, *TcDuox* was additionally expressed in

377 the *Duox* knockdown flies (*Rsl>NIG3131R-3*). With the expression of *TcDuox*, the

378 jump distance was increased to around twofold that of the *Duox* knockdown flies

379 (Figure 5E), indicating that *TcDuox* expression compensated for the reduction in the

380 level of the endogenous *Duox* expression.

381

382 **Discussion**

383 Duox is the oxidase that is widely conserved in metazoans, and is known as the thyroid

384 oxidase in mammals[43,44]. There have been many studies on the diverse roles of Duox,

385 including defense responses against intestinal wounds, immune responses against

386 pathogens, the regulation of stem cell development/differentiation, and extracellular

387 matrix formation[37-40,45-48]. In particular, in ecdysozoans such as insects and nematodes,

388 it is considered that the Duox-mediated crosslinking through dityrosine formation is

389 very important for the strengthening and stabilization of the extracellular matrix[37-39,49].

390 In this study, we showed that Rsl was polymerized by Duox, in which inter-Rsl

391 molecule dityrosine formation may occur (Figures 4C, 4D, 4H, and 4J). In insects, this

392 is the first study to identify the target protein of the Duox-mediated polymerization.

393 The polymerization of Rsl may be used as a model to study the formation of the

394 dityrosine matrix, which is distributed widely in metazoan taxa, including annelids and

395 molluscs[50,51].

396 Until this study, two reports on the function of the resilin-encoding gene in

397 Drosophilae species had been published, both by Moussian's group. Here, we were

398 able to specify the internal structures related to the emergence of this phenotype

399 (Figure 3F). As shown in Figure 3F, the tergopleural tendon was ruptured in Rsl^{KO} flies.

400 The direct flight muscles (TP-1 and TP-2) that are linked to the tergopleural tendon are

401 required for the movement of the wings that are upturned, as has been demonstrated in

402 a neurogenetic experiment[52]. Probably, in the *Rsl* knockdown and Rsl^{KO} flies, the

403 tergopleural tendon may have been damaged owing to the accumulation of stress from

404 the wing movement, since the occurrence of this phenotype is time-dependent (Figures

405 3B and 3D). After the rupture of the tergopleural tendon, energy transfer from the

406 muscle to the wings may no longer occur.

407 In the insect database of the full-length CDS or long-read RNA-seq results, we

408 found two splicing isoforms of resilins with or without the chitin-binding domain (our

409 observation), which indicates the possibility that the presence of these two isoforms is

410 important. The localization of Rsl-PA::mCherry (with the chitin-binding domain) in the

411 tergopleural tendon (Figure 2H) is actually similar to that observed in the distribution

412 of chitin fibers that were visualized using the ChtVis-tdTomato chitin reporter (Figure

413 2I). This suggests that the chitin-binding domain of Rsl-PA is functional *in vivo*, which

414 is consistent with the finding of an *in vitro* experiment using recombinant Rsl, showing

415 the binding of the chitin-binding domain to chitin[23]. The binding of the Rsl molecule to

416 chitin fibers seems to have a certain significance for the formation and proper

417 functions of the tergopleural tendon. However, when we compared the extent of

418 phenotypic rescue by overexpressions of *Rsl-RA* and *Rsl-RB* in Rsl^{KO} flies, the

419 downturned wing phenotypes were rescued, in almost the same proportion (Figure 3D).

420 This suggests that the chitin-binding domain is not necessarily required for Rsl

421 functions at the wing hinge. In the wing hinge, it is possible that other cuticle proteins

422 with both tyrosine residues and the chitin-binding domain may compensate for the

423 absence of the chitin-binding ability of Rsl-PB by mediating the linkage between chitin

424 fibers and Rsl-PB.

425 The polymerization of elastic protein moieties often occurs to give the matrix

426 high elasticity, as seen in other elastic materials, such as elastin and abductin[53-55]. *In*

427 *vitro* experiments designed to polymerize recombinant Rsls support this theory[5,20,53]. In

428 these studies, either peroxidase, photocatalysts, or chemical modifiers were used to

429 artificially polymerize Rsl, and the resulting materials treated with these reagents

430 exhibited high elasticity. The representative molecule forming the elastic matrix in

431 mammals is elastin, which is referred to as the "molecular spring" because of its roles

432 in restoring the structure and providing elasticity to tissues[53-55]. The tyrosine residues

433 of Rsl may form intermolecular crosslinks, which may be responsible for the formation

434 of the resilin matrix and its high resilience. According to the UniProt website

435 (https://www.uniprot.org/uniprotkb/Q9V7U0/entry), the chitin-binding domain of the
436 resilin model has a pLDDT score greater than 90, indicating high precision in the 3D
437 model prediction. However, the scores for the N- and C-terminal repeats are estimated
438 to be low (pLDDT score <70), which indicates that these regions could be intrinsically
439 disordered proteins. This is consistent with previous predictions that the Rsl molecule
440 has a random structure, lacking alpha helices or beta sheets[23,56]. However, low scores
441 in AlphaFold's predictions may simply reflect insufficient information about proteins
442 possessing similar sequences that could serve as references for known protein
443 structures during 3D modeling. At present, there is insufficient evidence to rule out the
444 possibility that Rsl possesses a structure similar to that of the predicted model. To
445 accurately understand the thermodynamic mechanism by which polymerized Rsl
446 molecules exhibit high elasticity, it would be beneficial to confirm whether Rsl
447 actually possesses a coil-like structure.

448 As shown in Figure 4A, the knockdown of *Duox* induced the same downturned
449 wing posture as that of the *Rsl* mutant. This result can be explained by the failure of
450 Rsl polymerization, as shown in the western blot in Figure 4C. Even in the adult stage,

451 Rsl polypeptides remained detectable at an electrophoretic mobility corresponding to
452 those of the Rsl monomers. *Duox* knockdown also induced the reduction in the
453 intensity of dityrosine signal in the tergopleural tendon (Figure 4I), strongly supporting
454 the idea that Duox is the factor for dityrosine-mediated Rsl polymerization. The
455 reduction or loss of the elasticity of the resilin matrix at the tergopleural tendon may
456 have occurred, finally leading to the rupture of the tergopleural tendon. It is also
457 possible that the link between the tergopleural tendon and the muscle is lost, probably
458 because of the weak bonding between them, as can be assumed from the detachment of
459 the muscle from the tergopleural tendon (Figure 4E).

460 The model that Duox is the factor for Rsl polymerization was based on the
461 studies of the nematode *Caenorhabditis elegans*, showing that the gene for Duox is
462 involved in the dityrosine-mediated polymerization of collagens in the cuticle
463 matrix[38,49]. It is possible that this process may be controlled by humoral factors,
464 because it is stage-dependent (Figure 2B). It has been shown that the functions of
465 Duox are regulated by the EF-hand motif present at the intracellular part of this
466 protein[40,45]. We observed an increase in the cytosolic calcium level in the cells

467 surrounding the tergopleural tendon in the late pupal stages (our observation). The next
468 step is to clarify whether the increase in the cytoplasmic calcium level actually
469 contributes to the activation of Duox and the subsequent dityrosine formation,
470 followed by elucidation of the molecular mechanisms underlying the stage-dependent
471 regulation of Rsl polymerization during the process of adult development.

472 Regarding jumping, both *Rsl*^{KO} and *Duox* knockdown flies showed shortened
473 jump distances, suggesting the loss of the polymerized Rsl may have been the cause of
474 this phenotype (Figure 5). In a recent study on the resilin gene of the locust *S. gregaria*,
475 the authors showed the lower jump performance of RNAi individuals (reduced jump
476 velocity and irreversible reduction in the jump distance during repetitive jumps)[57]. It
477 was also shown that the joints of the hind legs (between the femur and the tibia) were
478 more easily broken in the RNAi individuals. In *D. melanogaster*, the resilin matrix is
479 present on the ventral side of the leg joint (Figure 2); from the finding, we proposed a
480 simple model on how the resilin matrix works in fly jumping (Figure S10). Before
481 jumping, the resilin matrix becomes tense to store mechanical energy, and when the fly
482 jumps, the stored energy may be liberated from the resilin matrix during transition to

483 its relaxed state.

484 As shown in the observation of the *Rsl*^{KO} flies, we found the wing structures still

485 showing blue fluorescence (Figure S8). The lack of Rsl is also supported by the

486 previous observation that there are no reporter signals at the proximal part of the

487 wing[21]. In many reports, the term 'resilin' has been used to refer to the cuticular or

488 other extracellular structures with blue fluorescence. However, the data from *Rsl*^{KO}

489 flies show the existence of the non-resilin matrix with dityrosine, indicating that the

490 matrices positive for blue fluorescence do not necessarily contain Rsl molecules. It is

491 possible that such the non-resilin matrix with blue fluorescence may have mechanical

492 properties quite different from those of the resilin matrix, because blue fluorescence

493 can be found in very hard parts such as the tip of the mandible of copepods or

494 ragworm[58,59]. Future studies will reveal the mechanical characteristics or composition

495 of the non-resilin matrix with blue fluorescence and the biological significance of their

496 existence.

497 **Materials and Methods**

498 **Fly stocks and maintenance**

499 Fly stocks were reared at 25°C under a 12h light and dark cycle. They were fed the

500 standard cornmeal‑agar‑glucose medium containing propionic acid and n-butyl

501 p-hydroxybenzoate (7.21% cornmeal, 3.20% glucose, 8.01% yeast, and 0.64% agar

502 supplemented with 9.9 mL/L butyl *p*-hydroxybenzoate and 3.0 mL/L propionic acid) .

503 w^{1118} (our laboratory stock, Canton-S background) was used as the wild-type strain.

504 *UAS-eGFP* (BL#1521), *UAS-GFP-RNAi* (BL#9331), *vas-int* (BL#40161), AttP2

505 (BL#36303), AttP5 (BL#34766), and *vas-Cas9* (BL#51323) were obtained from the

506 Bloomington Drosophila Stock Center. *UAS-resilin-RNAi* (*KK106773*) in VIE260b

507 (#101068) was obtained from the Vienna Drosophila Resource Center. *UAS-Duox-RNAi*

508 (#3131R-3) and $y^2cho^2v^1$*; Sco/CyO* (#TBX-0007) were obtained from Fly Stocks of the

509 National Institute of Genetics. *UAS-Duox-RNAi*$_{976–1145}$[40] was kindly provided by Dr.

510 Won-Jae Lee (Seoul National University, Korea). All mutants and lines that were used

511 for knockdown were crossed into the w^{1118} control background for at least five

512 generations.

513

514 **RNA isolation and reverse-transcription PCR**

515 Total RNA was extracted from individuals at each growth stage using RNAiso Plus

516 (D9108A, Takara, Japan). cDNA was synthesized from 1 μg of total RNA using Prime

517 Script RT Reagent Kit with gDNA Eraser (DRR047A, Takara). cDNAs were amplified

518 using Prime star Max (R045A, Takara). To obtain patterns of stage-specific gene

519 expressions, a three-step thermal cycling profile was used as follows: 95 °C for 1 min,

520 followed by 25 cycles at 98 °C for 10 s, 55 °C for 5 s, and 72 °C for 5 s. The primers

521 used in the RT-PCR are listed in Supplementary Table 1.

522

523 **Generation of fly strains**

524 *Rsl*^{KO} was obtained by the CRSPR/Cas9-mediated deletion of the whole coding region

525 with two gRNAs[60]. The gRNAs were expressed from a transgene with a ubiquitous *pol*

526 *III* promoter derived from *Drosophila snRNA:U6:96Ab*[61]. For construction of DNA to

527 generate flies expressing gRNAs, two primer sets for *Rsl-gRNA1* and *-gRNA2* (listed in

528 Supplementary Table 2) were annealed, and the resulting DNA fragments were

529 separately subcloned into *pBFv-U6.2* and *pBFv-U6.2B*, respectively, that were

530 predigested with *Bbs*I. *pBFv-U6.2* with the sequence of *Rsl-gRNA1* was digested with

531 *EcoR*I and *Not*I, and one of the resulting DNA fragments (with the sequence of

532 *Rsl-gRNA1*) was ligated into one of the *EcoR*I and *Not*I fragment of *pBFv-U6.2B* (with

533 the sequence of *Rsl-gRNA2*). The resulting vector with both the sequences for

534 expressing *Rsl-gRNA1* and *-gRNA2* was introduced into AttP2 flies using a phiC31

535 integration system[60,61]. The flies with the transgene were crossed with *vas-Cas9* flies

536 and the offspring were crossed with $y^2cho^2v^1$*; Sco/CyO* virgins to establish lines with

537 deletions. The genotypes of the established lines were checked by genomic PCR

538 analysis using the primers listed in Supplementary Table 2.

539 For the construction of the plasmid vector for generating transgenic flies

540 (*Rsl-Gal4, Rsl* genomic rescue (*Rsl*-GR)*, UAS-Rsl-RA*, and *UAS-Rsl-RB*), genomic

541 DNA and cDNA obtained from w^{1118} were used as templates of PCR. For the subcloning

542 of the PCR fragments, an In-Fusion HD cloning kit (Z9648N, Takara) was used. To

543 construct the vector of *Rsl-Gal4*, the 2.3 kbp PCR fragment for the *Rsl* promoter region

544 amplified using the primer set (Supplementary Table 2) was subcloned into *pBPGw*

545 (Addgene; https://www.addgene.org/) that was predigested with *Kpn*I and *Bgl*II. To

546 generate flies with the transgene for the genomic rescue of Rsl^{KO}, we prepared a 4.7 kb

547 genomic fragment containing the *Rsl* CDS (from 1.0 kb upstream to 0.5 kb downstream

548 of the transcription start and stop sites of *Rsl*) which was amplified by PCR using the

549 primer set (Supplementary Table 2). The DNA fragment was subcloned into *pBFv-U6.2*

550 predigested with *EcoR*I and *Not*I. For the construction of the plasmid vector to generate

551 *UAS-Rsl-RA* and *UAS-Rsl-RB*, PCR fragments corresponding to the whole coding

552 regions of *Rsl-RA* and *Rsl -RB,* respectively, were amplified using the primer set

553 (Supplementary Table 2) with the cDNA. They were subcloned into *pUAST-attB*

554 (laboratory stock) predigested with *Not*I and *Xba*I. For the construction of the vector for

555 *UAS-TcDuox*, the DNA fragment corresponding to the whole coding region of the duox

556 gene of the red flour beetle *Tribolium castaneum* was amplified by PCR using the *T.*

557 *castaneum* cDNA and the primer set (Supplementary Table 2) (*T. castaneum* was a kind

558 gift from Dr. Toru Togawa, Nihon University, Japan). For the construction of

559 *UAS-Rsl-RA::mCherry* and *UAS-Rsl-RB::mCherry*, the whole coding region of each

560 isoform was amplified by PCR using the primer set (Supplementary Table 2) with

561 cDNA from iso-1 (BL2057) as the template. A fragment including the sequence of

562 mCherry with an N-terminal flexible 4 × GlyGlySer linker was PCR-amplified from

563 *UASp-Elyssim-mCherry*[62] using the primer set (Supplementary Table 2). The two DNA

564 fragments were subcloned into *EcoR*I fragment of *pUAST-attB* by the SLiCE method

565 (Motohashi, 2015). Each vector was introduced into flies with AttP5 (*UAS-Rsl-RA,*

566 *UAS-Rsl -RB,* and *UAS-Tcduox*) or AttP2 (*Rsl-Gal4*, *Rsl-GR, UAS-Rsl-RA::mCherry*,

567 and *UAS-Rsl-RB::mCherry*) using a phiC31-based integration system[63,64].

568

569 **Generation of antibody**

570 A part of Rsl (Lys478-Gly590) was chosen as the antigen to raise the antibody against

571 Rsl. In this study, pET-32 (Novagen, USA) was used to express the Rsl antigen as a

572 fusion protein with the N-terminally located thioredoxin. The DNA fragment

573 corresponding to the antigen was amplified with the primer set (Supplementary Table 1)

574 using the cDNA of w^{1118}. The PCR product was digested with *Xho*I and *Bgl*II, and

575 ligated into pET-32 predigested with the same enzyme set. The vector constructed was

576 used to transform the *E. coli* BL21 strain. After the IPTG induction of the recombinant

577 protein expression (1 mM, 4 h of culture at 37°C), the *E. coli* cells were harvested by

578 centrifugation, and ruptured by sonication in 50 mM Tris-HCl (pH 7.5) containing 150

579 mM sodium chloride. From the extract, the recombinant protein was purified by

580 Ni-NTA affinity chromatography using Ni-NTA Agarose (30210, Qiagen, Germany).

581 The N-terminally located thioredoxin was removed by thrombin treatment () to break

582 the peptide bond between the thioredoxin and the Rsl antigen, and the Rsl antigen was

583 used for the immunization of a rabbit. The serum obtained from the rabbit was used as

584 the anti-Rsl antibody.

585

586 **Western blot analysis of fly samples**

587 Five individuals at different stages (white pupae, pupae, and adults) were homogenized

588 in 400 μL of 2×SDS-PAGE sample buffer (12.5 mM Tris at pH 6.8, 20% glycerol, 4%

589 SDS, 2% 2-mercaptoethanol, and 0.001% bromophenol blue) and boiled for 10 min at

590 100°C. The proteins in a 5 μL aliquot were separated by SDS-PAGE using 12.5%

591 polyacrylamide gel and transferred to PVDF membranes (IPFL00010, Merck KGaA,

592 Germany). After blocking using 5% skim milk with TBST (0.1% Tween20), the

593 membranes were incubated with the rabbit anti-Rsl antibody (1: 3000 dilution) and

594 mouse anti- α -Tubulin antibody [DM1A] (ab7291, Abcam, UK) (1: 5000 dilution) in

595 Can Get signal solution 1 (NKB-201, Toyobo, Japan) at 4°C overnight. For the

596 secondary antibody, IRDye-conjugated anti-rabbit and anti-mouse IgGs (925-68071 and

597 925-32210, respectively, LI-COR, USA) were used with Can Get signal solution 2

598 (NKB-301, TOYOBO, Japan) (1: 20000 dilution, for 2 h at 25°C). For luminescence

599 imaging, an Odyssey DLx imaging system (LI-COR, USA) was used.

600

601 **Measurement of jump distance**

602 One day before the experiments, the flies were de-winged under mild CO_2 anesthesia.

603 Jump distance was measured using the equipment, which was set in a room kept as

604 25°C. At the bottom of the glass beaker, 2% agarose was placed. After hardened, the

605 agarose solution, a mesh for scaling was put on the agarose gel, and the surface was

606 covered with additional 2% agarose. Five flies per group were housed in the equipment

607 and their jumping were tracked for 5 minutes at 480 fps with Tough TG-5

608 (4545350-051112, OLYMPUS, Japan) and the jump distances were measured on the

609 basis of intervals of the mesh. The longest jump distance in each group was used as the

610 representative value. The experiments were performed at least eight times for each

611 genotype and sex.

612

613 **Crosslinking of Rsl**

614 Horseradish peroxidase was used for the crosslinking reaction of recombinant Rsl[21,65].

615 100 μg of the recombinant Rsl (CSB-EP892693DLU, WUHAN HUAMEI BIOTECH,

616 USA) was dissolved with 100 μl of 50 mM potassium phosphate buffer (pH7.0).

617 Horseradish peroxidase (P-8375, Sigma, USA) was dissolved with 0.1 M potassium

618 phosphate buffer (pH 6.0) to a final concentration of 20 μg/μL. 1 μL of the recombinant

619 Rsl solution was mixed with 5 μL of 50 mM potassium phosphate buffer (pH 7.0). Then,

620 1 μL of horseradish peroxidase solution and 3 μL of 0.3% hydrogen peroxide (18084-00,

621 KANTO CHEMICAL, Japan) were added, and the mixture was incubated at 30°C for 1

622 h. After incubation, the reaction mixture was mixed with 10 μL 2×SDS-sample buffer

623 and boiled for 10 min at 100°C. Western blot analyses of Rsl and dityrosine were

624 performed using the rabbit anti-Rsl antibody (this study) and the mouse monoclonal

625 anti-dityrosine antibody (MDT-020P, JaICA, Japan). The experimental procedures of

626 western blot analysis were the same as those described in section 2.5.

627

628 **Histology and microscopy**

629 To observe the internal structure of the wing hinge, the adult thorax was divided into

630 two parts (left and right) along the midline. Then the body parts around the wing hinge

631 were obtained by trimming with microscissors. The tissues were fixed using 4%

632 paraformaldehyde with PBS (pH 7.0). After blocking using 5% BSA (A7906, Merck

633 KGaA) with PBST (0.05% Tween20), these samples were incubated in

634 phaloidin-iFluor488 (CAY20549, Cayman Chemical, USA) with PBST (1:500) at 25°C

635 overnight. An OLYMPUS BX60 (OLYMPUS, Japan) equipped with an

636 WRAYCAM-VEX830 (WRAYMER, Japan) was used for whole-body or dityrosine,

637 mCherry, and YFP signal detection. An OLYMPUS SZX7 (OLYMPUS, Japan)

638 equipped with an OLYMPUS DP71 (OLYMPUS, Japan) was used for observing the

639 phenotypes of wing posture.

640

641 **Quantification of biased Rsl::mCherry distribution**

642 The standard deviation (std) and the mean intensity of the mCherry signal in the resilin

643 matrix were quantified using ImageJ. The std/mean was used as the index of the biased

644 Rsl::mCherry distribution[66].

645

646 **Statistical analyses**

647 Statistical analyses were performed using R version 3.6.0 (https://www.r-project.org/).

648 The Wilcoxon rank sum test was used to compare the jump distances. The student t-test

649 was used to compare the intensities of mCherry signals in the resilin matrix in the wing

650 hinges. The Steel‑Dwass test was used to compare the expression levels of *Rsl*, *Duox,*

651 and *TcDuox*.

652

653 **Acknowledgements**

654 *UAS-Duox-RNAi*$_{976–1145}$ was a kind gift of Dr. Won-Jae Lee (Seoul National University,
655 Korea). *T. castaneum* was a kind gift from Dr. Toru Togawa (Nihon University, Japan).
656 We are grateful to Mr. Kensuke Aizawa for his contributions to our preliminary
657 experiments in the early period. We thank the National Institute of Genetics, the
658 University of Indiana. Bloomington *Drosophila* Stock Center and the Vienna
659 *Drosophila* Resource Center for providing fly lines. This work is supported by JSPS
660 KAKENHI Grant Number JP23H02225 and 21J21904 and the Sasakawa Scientific

Research Grant from The Japan Science Society.

Author contributions

M.H. and T.Asa. initiated, designed the experiments, and developed the project. M.H. performed all the experiments, analyzed the data, and prepared the figures. Y.E. and Y.K. generated *UASt-resilin-RA::mCherry* and *UASt-resilin-RB::mCherry*. M.H. and T.Asa. wrote and edited the manuscript. H.O.I., T.S., T.A. and T.Asa. reviewed the manuscript.

Competing interests

The authors declare no competing financial interests.

References

1. Ellington, C. P. The aerodynamics of hovering insect flight. VI. Lift and power requirements. *Philos. Trans. R. Soc. London. B, Biol. Sci.* **305**, 145–181 (1984).
2. Ellington, C. P. Power and efficiency of insect flight muscle. *J. Exp. Biol.* **VOL. 115**, (1985).
3. Andersen, S. O. & Weis-Fogh, T. Resilin. A Rubberlike Protein in Arthropod Cuticle. *Adv. In Insect Phys.* **2**, 1–65 (1964).
4. Weis-Fogh, T. A Rubber-Like Protein in Insect Cuticle. *J. Exp. Biol.* **37**, (1960).
5. Elvin, C. M. *et al.* Synthesis and properties of crosslinked recombinant pro-resilin. *Nature* **437**, 999–1002 (2005).
6. Parry, D. A. & Brown, R. H. J. The Hydraulic Mechanism of the Spider Leg. *J. Exp. Biol.* **36**, 423–433 (1959).
7. Wan, C., Hao, Z. & Feng, X. Structures, properties, and energy-storage mechanisms of the semi-lunar process cuticles in locusts. *Sci. Reports 2016 61* **6**, 1–13 (2016).
8. Wan, C. & Gorb, S. N. Body-catapult mechanism of the sandhopper jump and its biomimetic implications. *Acta Biomater.* **124**, 282–290 (2021).
9. Burrows, M. Development and deposition of resilin in energy stores for locust jumping. *J. Exp. Biol.* **219**, 2449–2457 (2016).
10. Sutton, G. P. & Burrows, M. Biomechanics of jumping in the flea. *J. Exp. Biol.* **214**, 836–847 (2011).
11. Bennet-Clark, H. C. Negative Pressures Produced in the Pharyngeal Pump of the Blood-Sucking Bug, Rhodnius Prolixus. *J. Exp. Biol.* **40**, 223–229 (1963).
12. Young, D. & Bennet-Clark, H. C. The Role of the Tymbal in Cicada Sound Production. *J. Exp. Biol.* **198**, 1001–1020 (1995).
13. Lyons, R. E. *et al.* Molecular and functional characterisation of resilin across three insect orders. *Insect Biochem. Mol. Biol.* **41**, 881–890 (2011).
14. Stutt, A. D. & Siva-Jothy, M. T. Traumatic insemination and sexual conflict in the bed bug Cimex lectularius. *Proc. Natl. Acad. Sci. U. S. A.* **98**, 5683–5687 (2001).
15. Michels, J., Gorb, S. N. & Reinhardt, K. Reduction of female copulatory damage by resilin represents evidence for tolerance in sexual conflict. *J. R. Soc. Interface* **12**, (2015).
16. McKenzie, E. K. G., Kwan, G. T., Tresguerres, M. & Matthews, P. G. D. A pH-powered mechanochemical engine regulates the buoyancy of Chaoborus midge larvae. *Curr. Biol.* **32**, 927-933.e5 (2022).

705 17. Andersen, S. O. The cross-links in resilin identified as dityrosine and trityrosine. *BBA - Gen. Subj.*
706 **93**, (1964).
707 18. Ardell, D. H. & Andersen, S. O. Tentative identification of a resilin gene in Drosophila
708 melanogaster. *Insect Biochem. Mol. Biol.* **31**, 965–970 (2001).
709 19. Balu, R., Dutta, N. K., Dutta, A. K. & Choudhury, N. R. Resilin-mimetics as a smart biomaterial
710 platform for biomedical applications. *Nat. Commun. 2021 121* **12**, 1–15 (2021).
711 20. Li, L. & Kiick, K. L. Resilin-based materials for biomedical applications. *ACS Macro Lett.* **2**,
712 635–640 (2013).
713 21. Qin, G. *et al.* Recombinant exon-encoded resilins for elastomeric biomaterials. *Biomaterials* **32**,
714 9231–9243 (2011).
715 22. Lerch, S. *et al.* Resilin matrix distribution, variability and function in Drosophila. *BMC Biol.* **18**,
716 1–15 (2020).
717 23. Ohkubo, S., Shintaku, T., Mine, S., Yamamoto, D. S. & Togawa, T. Mosquitoes Possess
718 Specialized Cuticular Proteins That Are Evolutionarily Related to the Elastic Protein Resilin.
719 *Insects* **14**, 941 (2023).
720 24. Andersen, S. O. Studies on resilin-like gene products in insects. *Insect Biochem. Mol. Biol.* **40**,
721 541–551 (2010).
722 25. Abramson, J. *et al.* Accurate structure prediction of biomolecular interactions with AlphaFold 3.
723 *Nature* **630**, 493–500 (2024).
724 26. Lerch, S., Yang, Y., Flaven-Pouchon, J., Gehring, N. & Moussian, B. Resilin is needed for wing
725 posture in Drosophila suzukii. *Arch. Insect Biochem. Physiol.* **111**, e21913 (2022).
726 27. Neff, D. Bursicon, Metamorphosis and Development of Resilin in the Fruit Fly. *Theses, Diss.*
727 *Capstones* (2012).
728 28. Wong, D. C. C., Pearson, R. D., Elvin, C. M. & Merritt, D. J. Expression of the rubber-like
729 protein, resilin, in developing and functional insect cuticle determined using a Drosophila anti-rec
730 1 resilin antibody. *Dev. Dyn.* **241**, 333–339 (2012).
731 29. Fabian, B., Schneeberg, K. & Beutel, R. G. Comparative thoracic anatomy of the wild type and
732 wingless (wg1cn1) mutant of Drosophila melanogaster (Diptera). *Arthropod Struct. Dev.* **45**,
733 611–636 (2016).
734 30. Dietzl, G. *et al.* A genome-wide transgenic RNAi library for conditional gene inactivation in
735 Drosophila. *Nat. 2007 4487150* **448**, 151–156 (2007).
736 31. Greene, J. C. *et al.* Mitochondrial pathology and apoptotic muscle degeneration in Drosophila
737 parkin mutants. *Proc. Natl. Acad. Sci. U. S. A.* **100**, 4078–4083 (2003).

738 32. Park, J. *et al.* Mitochondrial dysfunction in Drosophila PINK1 mutants is complemented by
739 parkin. *Nature* **441**, 1157–1161 (2006).
740 33. Michels, J., Appel, E. & Gorb, S. N. Functional diversity of resilin in Arthropoda. *Beilstein*
741 *Journal of Nanotechnology* (2016) doi:10.3762/bjnano.7.115.
742 34. Appel, E., Heepe, L., Lin, C. P. & Gorb, S. N. Ultrastructure of dragonfly wing veins: Composite
743 structure of fibrous material supplemented by resilin. *J. Anat.* **227**, 561–582 (2015).
744 35. Michels, J. & Gorb, S. N. Detailed three-dimensional visualization of resilin in the exoskeleton of
745 arthropods using confocal laser scanning microscopy. *J. Microsc.* **245**, 1–16 (2012).
746 36. Gidaszewski, N. A., Baylac, M. & Klingenberg, C. P. Evolution of sexual dimorphism of wing
747 shape in the Drosophila melanogaster subgroup. *BMC Evol. Biol.* **9**, 1–11 (2009).
748 37. Anh, N. T. T., Nishitani, M., Harada, S., Yamaguchi, M. & Kamei, K. Essential role of duox in
749 stabilization of Drosophila wing. *J. Biol. Chem.* (2011) doi:10.1074/jbc.M111.263178.
750 38. Edens, W. A. *et al.* Tyrosine cross-linking of extracellular matrix is catalyzed by Duox, a
751 multidomain oxidase/peroxidase with homology to the phagocyte oxidase subunit gp91phox. *J.*
752 *Cell Biol.* (2001) doi:10.1083/jcb.200103132.
753 39. Hurd, T. R., Liang, F. X. & Lehmann, R. Curly Encodes Dual Oxidase, Which Acts with Heme
754 Peroxidase Curly Su to Shape the Adult Drosophila Wing. *PLOS Genet.* **11**, e1005625 (2015).
755 40. Ha, E. M., Oh, C. T., Bae, Y. S. & Lee, W. J. A direct role for dual oxidase in Drosophila gut
756 immunity. *Science (80-.).* **310**, 847–850 (2005).
757 41. Burrows, M., Shaw, S. R. & Sutton, G. P. Resilin and chitinous cuticle form a composite
758 structure for energy storage in jumping by froghopper insects. *BMC Biol.* **6**, 1–16 (2008).
759 42. Burrows, M. & Sutton, G. P. Locusts use a composite of resilin and hard cuticle as an energy
760 store for jumping and kicking. *J. Exp. Biol.* **215**, 3501–3512 (2012).
761 43. De Deken, X. *et al.* Cloning of Two Human Thyroid cDNAs Encoding New Members of the
762 NADPH Oxidase Family. *J. Biol. Chem.* **275**, 23227–23233 (2000).
763 44. Dupuy, C. *et al.* Purification of a novel flavoprotein involved in the thyroid NADPH oxidase.
764 Cloning of the porcine and human cDNAs. *J. Biol. Chem.* (1999) doi:10.1074/jbc.274.52.37265.
765 45. Ha, E. M. *et al.* Coordination of multiple dual oxidase–regulatory pathways in responses to
766 commensal and infectious microbes in drosophila gut. *Nat. Immunol. 2009 109* **10**, 949–957
767 (2009).
768 46. Lee, K. A. *et al.* Bacterial-derived uracil as a modulator of mucosal immunity and gut-microbe
769 homeostasis in drosophila. *Cell* **153**, 797–811 (2013).
770 47. Moreira, S., Stramer, B., Evans, I., Wood, W. & Martin, P. Prioritization of Competing Damage

and Developmental Signals by Migrating Macrophages in the Drosophila Embryo. *Curr. Biol.* **20**, 464–470 (2010).

48. Niethammer, P., Grabher, C., Look, A. T. & Mitchison, T. J. A tissue-scale gradient of hydrogen peroxide mediates rapid wound detection in zebrafish. *Nat. 2009 4597249* **459**, 996–999 (2009).

49. Thein, M. C. *et al.* Combined Extracellular Matrix Cross-linking Activity of the Peroxidase MLT-7 and the Dual Oxidase BLI-3 Is Critical for Post-embryonic Viability in Caenorhabditis elegans. *J. Biol. Chem.* **284**, 17549–17563 (2009).

50. Suderman, R. J., Dittmer, N. T., Kramer, K. J. & Kanost, M. R. Model reactions for insect cuticle sclerotization: Participation of amino groups in the cross-linking of Manduca sexta cuticle protein MsCP36. *Insect Biochem. Mol. Biol.* **40**, 252–258 (2010).

51. Kumar, S., Molina-Cruz, A., Gupta, L., Rodrigues, J. & Barillas-Mury, C. A peroxidase/dual oxidase system modulates midgut epithelial immunity in anopheles gambiae. *Science (80-.).* **327**, 1644–1648 (2010).

52. O'Sullivan, A. *et al.* Multifunctional Wing Motor Control of Song and Flight. *Curr. Biol.* **28**, 2705-2717.e4 (2018).

53. Carvajal, M. F. C. A. *et al.* Dynamics in natural and designed elastins and their relation to elastic fiber structure and recoil. *Biophys. J.* **120**, 4623–4634 (2021).

54. Jamhawi, N. M., Koder, R. L. & Wittebort, R. J. Elastin recoil is driven by the hydrophobic effect. *Proc. Natl. Acad. Sci. U. S. A.* **121**, e2304009121 (2024).

55. Trębacz, H. & Barzycka, A. Mechanical Properties and Functions of Elastin: An Overview. *Biomol. 2023, Vol. 13, Page 574* **13**, 574 (2023).

56. Qin, G., Hu, X., Cebe, P. & Kaplan, D. L. Mechanism of resilin elasticity. *Nat. Commun.* **3**, (2012).

57. Rogers, S. M. *et al.* RNAi of the elastomeric protein resilin reduces jump velocity and resilience to damage in locusts. *Proc. Natl. Acad. Sci. U. S. A.* **122**, e2415625121 (2025).

58. Michels, J., Vogt, J. & Gorb, S. N. Tools for crushing diatoms - Opal teeth in copepods feature a rubber-like bearing composed of resilin. *Sci. Rep.* **2**, 1–6 (2012).

59. Birkedal, H. *et al.* Halogenated veneers: Protein cross-linking and halogenation in the jaws of Nereis, a marine polychaete worm. *ChemBioChem* **7**, 1392–1399 (2006).

60. Kondo, S. & Ueda, R. Highly Improved gene targeting by germline-specific Cas9 expression in Drosophila. *Genetics* **195**, 715–721 (2013).

61. Wakiyama, M., Matsumoto, T. & Yokoyama, S. Drosophila U6 promoter-driven short hairpin RNAs effectively induce RNA interference in Schneider 2 cells. *Biochem. Biophys. Res. Commun.*

331, 1163–1170 (2005).

62. Hirai, K. *et al.* The Drosophila nucleoporin ELYS is required for parental chromosome arrangement at fertilization. *G3 Genes|Genomes|Genetics* **15**, 104 (2025).

63. Bischof, J., Maeda, R. K., Hediger, M., Karch, F. & Basler, K. An optimized transgenesis system for Drosophila using germ-line-specific φC31 integrases. *Proc. Natl. Acad. Sci. U. S. A.* **104**, 3312–3317 (2007).

64. Groth, A. C., Fish, M., Nusse, R. & Calos, M. P. Construction of transgenic Drosophila by using the site-specific integrase from phage phiC31. *Genetics* **166**, 1775–1782 (2004).

65. Qin, G. *et al.* Expression, cross-linking, and characterization of recombinant chitin binding resilin. *Biomacromolecules* **10**, 3227–3234 (2009).

66. Zhang, X. *et al.* Mechanoresponsive regulation of myogenesis by the force-sensing transcriptional regulator Tono. *Curr. Biol.* **34**, 4143-4159.e6 (2024).

67. Misof B. *et al*. Phylogenetics resolves the timing and pattern ofinsect evolution. Science, 346, No. 6210 (2014).

820 **Figure legends**

821 Figure 1. Exon–intron organization in the *Rsl* locus and protein structures of Rsl. (A)
822 The top is a schematic of the *Rsl* locus in the wild-type fly. Black and white boxes are
823 CDSs and UTRs, respectively. The exon compositions of the two isoforms are shown
824 below. The schematics below show the *Rsl* locus in Rsl^{KO} flies; the regions chosen to
825 generate the transgenes for the rescue experiments (*Rsl-GR*) and for the Gal4 driver
826 (*Rsl-Gal4*) are shown. The short bars indicate two gRNAs designed for the deletion of
827 CDS to generate Rsl^{KO} flies. (B) Domain-motif organization of Rsl isoforms are shown.
828 Each of the functional domain or consensus is shown below. Rsl-PB has a small portion
829 of the chitin-binding R&R consensus sequence (red box) encoded by the 5' part of exon
830 3. (C) The 3D model of Rsl-PA predicted in AlphaFold Server is shown. Panel a is the
831 whole Rsl-PA model. Blue and green parts are the N-terminal and C-terminal repeats,
832 respectively. In panels b and c, the N-terminal and C-terminal repeats are enlarged with
833 their proline and tyrosine residues illustrated by blue and purple colors, respectively. In
834 panel c, beta turns are indicated by closed arrowheads. Panels d and e show the views in
835 which two repeats are extracted from panels b and c, respectively, with schematics for

836 two cycles of their polypeptide backbones.

837

838 Figure 2. Temporal patterns of *Rsl* expression and spatial patterns of the reporter. (A)

839 RT-PCRs of *Rsl-RA* and *Rsl-RB* from embryo to day 5 adult are shown. (B) Western

840 blots of the Rsl protein from white pupa to day 5 adult are shown. In both A and B, FL,

841 WL, WP, P1-4, and A0-5 are the abbreviations of feeding larva, wandering larva, white

842 pupa, pupa days 1−4, and adult day 0−5, respectively. (C−H and J) Spatial distribution

843 of the Rsl-RA::mCherry reporter expressed with *Rsl-Gal4* is shown. (C) Panels a – c

844 show the views from dorsal, lateral, and ventral directions, respectively. Photos on the

845 left side were taken under white light. In each panel, white arrowheads indicate the

846 mCherry signals at the wing hinges, spiracles, or labrum. The dotted circle indicates the

847 outline of the compound eye. (D and E) The midleg of the flies (D) and the edge of the

848 wing (E) are shown. Photos of the mCherry signal and bright field were merged. Scale

849 bar: 50 µm. (F) The western blots of Rsl in the compound eyes dissected from day-3

850 pupae of the wild-type and Rsl^{KO} flies are shown. The electrophoretic mobilities of

851 Rsl-PA and Rsl-PB are indicated with arrowheads. (G) The Rsl-RA::mCherry

852 localization at the wing hinge is shown. The outer cuticle was removed together with

853 the wing (arrowhead) to observe the internal structure (panel h). In panel i, the area

854 enclosed in the square in panel h is enlarged. Scale bar: 500 µm. (H) Panel j is the

855 magnified view of the wing hinge of the fly expressing *Rsl-RA::mCherry*. Panel k is the

856 photo taken under UV radiation, and panel l is the merged photo of panels j and k. Scale

857 bar: 50 µm. (I) The distribution pattern of ChtVis-tdTomato that was expressed with

858 *Rsl-Gal4* is shown. Scale bar: 50 µm. In both H and I, the wavelengths of the filters

859 used for excitation and the detection of dityrosine are 330−385 and >420 nm,

860 respectively. (J) The biased distributions of Rsl::mCherry signals are compared. Panels

861 p and q are the photos of the resilin matrix visualized with Rsl-RA::mCherry and

862 Rsl-RB::mCherry, respectively. In panel r, the deviations of the biased distribution were

863 calculated as described in Materials and Methods.

864

865 Figure 3. Phenotypes of *Rsl* knockdown and mutant flies. (A) The wing postures of the

866 control fly (left: *Rsl>GFP-RNAi*) and *resilin* knockdown fly (right: *Rsl>Rsl-RNAi*) are

867 compared. Scale bar: 0.5 mm. (B) The proportion of flies with normal wing posture on

868 each day against the total number of flies is indicated (closed circles: *Rsl>GFP-RNAi*,

869 grey circles: *Rsl>Rsl-RNAi*). (C) The wing postures of wild-type (w^{1118}), Rsl^{KO} (w^{1118};

870 Rsl^{KO}), and rescued (w^{1118}; $resilin^{KO}$; *resilinGR*) flies are compared. Scale bar: 0.5 mm.

871 (D) The temporal changes in the proportion of flies with normal wing posture after

872 eclosion are shown. The fly genotypes are w^{1118} (closed circles), $resilin^{KO}$ (gray circles),

873 $resilin^{KO}$; *resilinGR* (open circles), $resilin^{KO}$; *resilin-Gal4* (closed triangles), $resilin^{KO}$,

874 *UAS-resilin-RA* (gray triangles), $resilin^{KO}$, *UAS-resilin-RB* (open triangles), $resilin^{KO}$,

875 *UAS-resilin-RA; resilin-Gal4* (closed squares), $resilin^{KO}$,*UAS-resilin-RB; resilin-Gal4*

876 (gray squares), and Rsl^{KO},*UAS-Rsl-RA*/Rsl^{KO},*UAS-Rsl-RB*; *Rsl-Gal4* (open squares). (E)

877 The middle (Direction A) is a schematic diagram of the wing hinge that is viewed from

878 the midline toward the wing (blue arrow in the dorsal view of the fly). The right

879 (Direction B) shows the wing hinge viewed from posterior to anterior direction (red

880 arrow in the dorsal view of the fly). Blue shows the tergopleural tendon, which connects

881 to the cuticle where the wing attaches (yellow arrowheads). Red indicates direct flight

882 muscles TP1 and TP2[52]. (F) The inner structure of the wing hinge in *Dpy-YFP* was

883 observed (panel a, left part), and its schematic is shown (right part). The red signals

884 indicate muscles stained with phalloidin. The blue signal corresponds to blue

885 fluorescence emitted upon UV irradiation. Green signals indicate Dpy-YFP. White

886 arrow heads indicate the cuticle structure beneath the wing hinge attached to the

887 proximal end of the tergopleural tendon. Panels b and c show the inner structures and

888 the illustrations of the wing hinge of Rsl^{KO} flies (with and without the downturned wing

889 phenotype, respectively). Panel d shows those of the Rsl^{KO} fly with *Rsl*-GR. In Figure

890 3F, the adults 72 h after eclosion were used for taking the photos, except for panel b for

891 which adults 0 h after eclosion were used. Yellow arrowheads indicate the internal

892 cuticle structure corresponding to the root of the wing hinge. White arrowheads indicate

893 the tergopleural tendon devoid of any blue fluorescence signal in Rsl^{KO} flies. Asterisks

894 indicate Dpy-YFP signals attached to flight muscles other than TP-1 and TP-2. Scale

895 bar: 50 µm.

896

897 Figure 4. Analyses of *Duox* functions in Rsl polymerization. (A) The wing postures of

898 the control (*Rsl>GFP-IR*) and *Duox* knockdown flies (*Rsl>NIG 3131R-3*, and

899 *Rsl>Duox-RNAi*$_{976–1145}$) are compared. Scale bar: 0.5 mm. (B) The temporal changes in

900 the proportions of flies with normal wing posture after eclosion are shown. The flies

901 used were the same as those in (A) (closed circles: *Rsl>GFP-RNAi*, grey closed circles:

902 *Rsl>NIG3131R-3*, and gray open circles: *Rsl>Duox-RNAi*$_{976–1145}$). (C) Western blot

903 analyses of Rsl protein levels were performed using samples from day-4-APF pupae to

904 day-2-after-eclosion adults. The left and right are flies of the control (*Rsl>GFP-RNAi*)

905 and *Duox* knockdown (*Rsl>NIG3131R-3*), respectively. (D) The possible model of

906 Duox-mediated Rsl polymerization (after Edens et. al., 2001[38]) (E) The inner structures

907 of the wing hinge in the two control flies, *Rsl-Gal4/+* (panel a) and *NIG3131R-3/+*

908 (panel b), are shown. The changes in the structure in the *Duox*-knockdown flies

909 (*Rsl>NIG3131R-3*) are shown (panels c and d). Panel e on the right is the schematic of

910 panels c and d. TP-1 and TP-2 muscles were stained with phalloidin. In

911 *Duox*-knockdown flies, the dotted line (panels c and d) indicates the outline of the

912 dityrosine signal corresponding to the weak blue fluorescence signal indicated by

913 triangles in the photo taken with a longer exposure time. Scale bar: 50 μm. (F) Wing

914 posture of the *Duox* knockdown fly (*Rsl>NIG3131R-3, eGFP*) and that of the *Duox*

915 knockdown fly with the additional *TcDuox* expression (*Rsl> NIG3131R-3, TcDuox*).

916 Scale bar: 0.5 mm. (G) Difference in the proportion changes of flies with normal wing

917 posture was compared between *Rsl> NIG3131R-3, eGFP* (gray circle) and

918 *Rsl>NIG3131R-3, TcDuox* (closed circle) flies. (H) Western blot analyses were

919 performed to examine the levels of the Rsl protein from day-4-APF pupae to

920 day-2-after-eclosion adults are shown. The left shows the *Duox*-knockdown individuals

921 (*Rsl>NIG3131R-3, eGFP*) and the right shows the rescued individuals

922 (*Rsl>NIG3131R-3, TcDuox*). (I) The photos and illustrations of the inner structure of the

923 wing hinge in *Duox*-knockdown (left panels) and rescued flies (right panels) are shown.

924 Scale bar: 50 μm (J) Western blot analyses of reRsl protein and dityrosine levels. reRsl

925 was incubated in the presence (+) or absence (-) of 20 μg/μL horseradish peroxidase

926 (HRP) and/or 0.3% hydrogen peroxide (H_2O_2) in 50 mM sodium phosphate buffer (pH

927 7.0) for 1 h at 30ºC. Closed arrowheads show the signals stacking at the entry site of the

928 concentration gels. The open arrowhead shows the signal stacking at the border between

929 the concentration and separation gels. Curly bracket shows smear signals in the stacking

930 gel.

931

932 Figure 5. Contributions of *Rsl* and *Duox* to fly's jumping. (A) Experimental scheme to

933 measure jump distance of de-winged flies. (B) The jump distances between the control

934 flies (*Rsl>GFP-RNAi*, white box) and *Rsl* knockdown flies (*Rsl>Rsl-RNAi*, gray box)

935 are compared. Cross marks indicate the average. (Wilcoxon rank sum test, **: $P < 0.01$,

936 *Rsl>GFP-RNAi*: n=8, *Rsl>Rsl-RNAi*: n=12). (C) The Rsl^{KO} phenotype of jump distance

937 was rescued with *Rsl-GR*. The flies used were the wild-type (w^{1118}, white box), Rsl^{KO}

938 (w^{1118}; Rsl^{KO}, gray box), and Rsl^{KO} with *Rsl-GR* (w^{1118}; Rsl^{KO}; *Rsl-GR*, dark gray box).

939 Cross marks indicate the average (Wilcoxon rank sum test, Bonferroni correction, w^{1118}:

940 n=10, Rsl^{KO}: n=10, Rsl^{KO} with *Rsl-GR*: n=11). (D) Effect of *Duox* knockdown on jump

941 performance was examined. The graph shows the jump distances of the control flies

942 (*Rsl>GFP-RNAi,* white box), the *Duox* knockdown flies (*Rsl> NIG 3131R-3*, indicated

943 by the light gray box, and *Rsl>Duox-RNAi*$_{976–1145}$ indicated by the gray box) (Wilcoxon

944 rank sum test, Bonferroni correction, *Rsl>GFP-RNAi*: n=9, *Rsl> NIG 3131R-3*: n=12,

945 *Rsl>Duox-RNAi*$_{976–1145}$: n=8). (E) The phenotype of *Duox* knockdown flies was rescued

946 by the additional expression of *TcDuox*. The graph shows the jump distances of the

947 *Duox* knockdown flies (*Rsl> NIG3131R-3, eGFP,* white box) and the flies with *TcDuox*

948 expression (*Rsl> NIG3131R-3, TcDuox*, gray box) (Wilcoxon rank sum test, **: $P <$

949 0.01, *Rsl> NIG3131R-3, eGFP*: n=9, *Rsl> NIG3131R-3, TcDuox*: n=7).

950

951

952 Figure 1

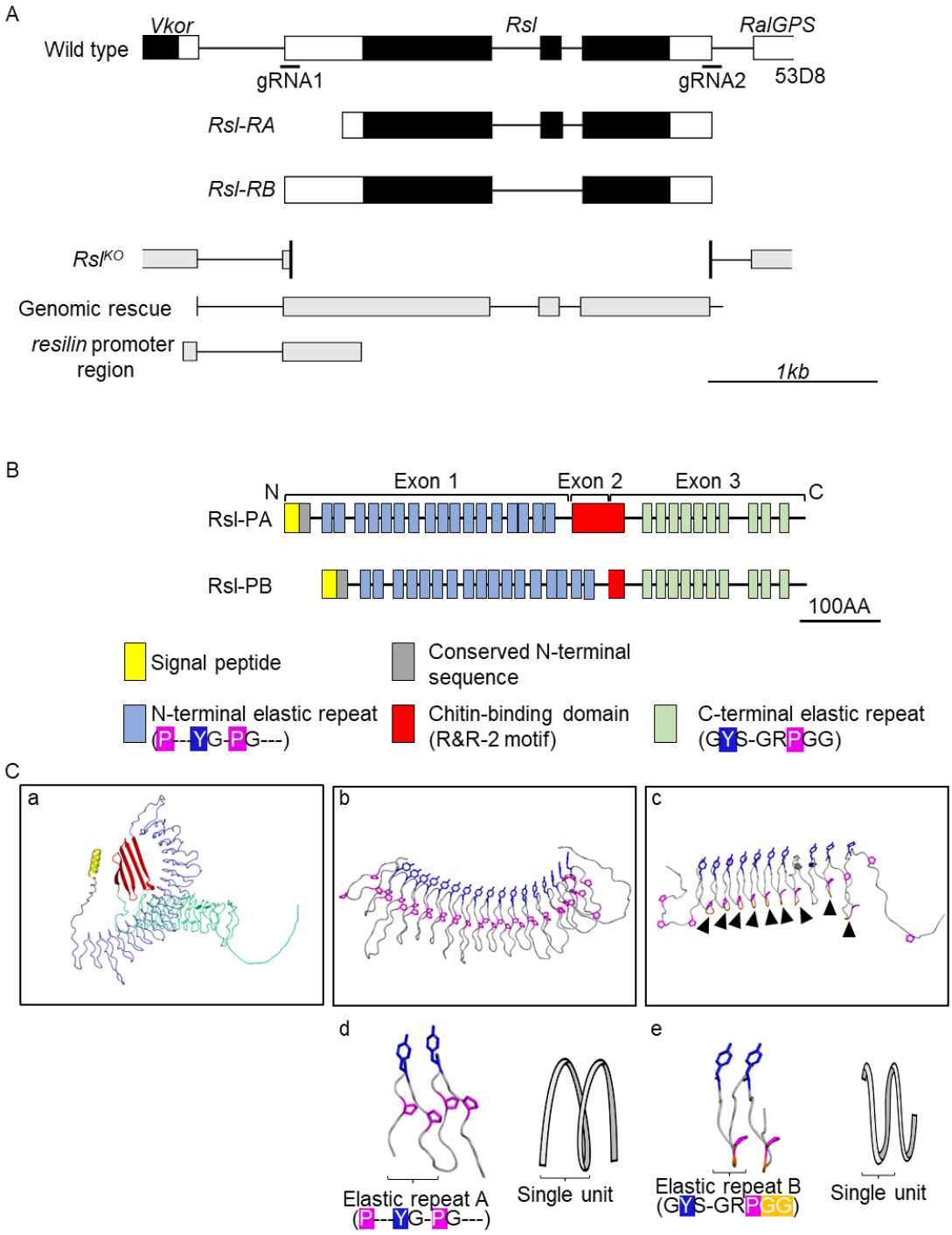

953
954

Figure 2

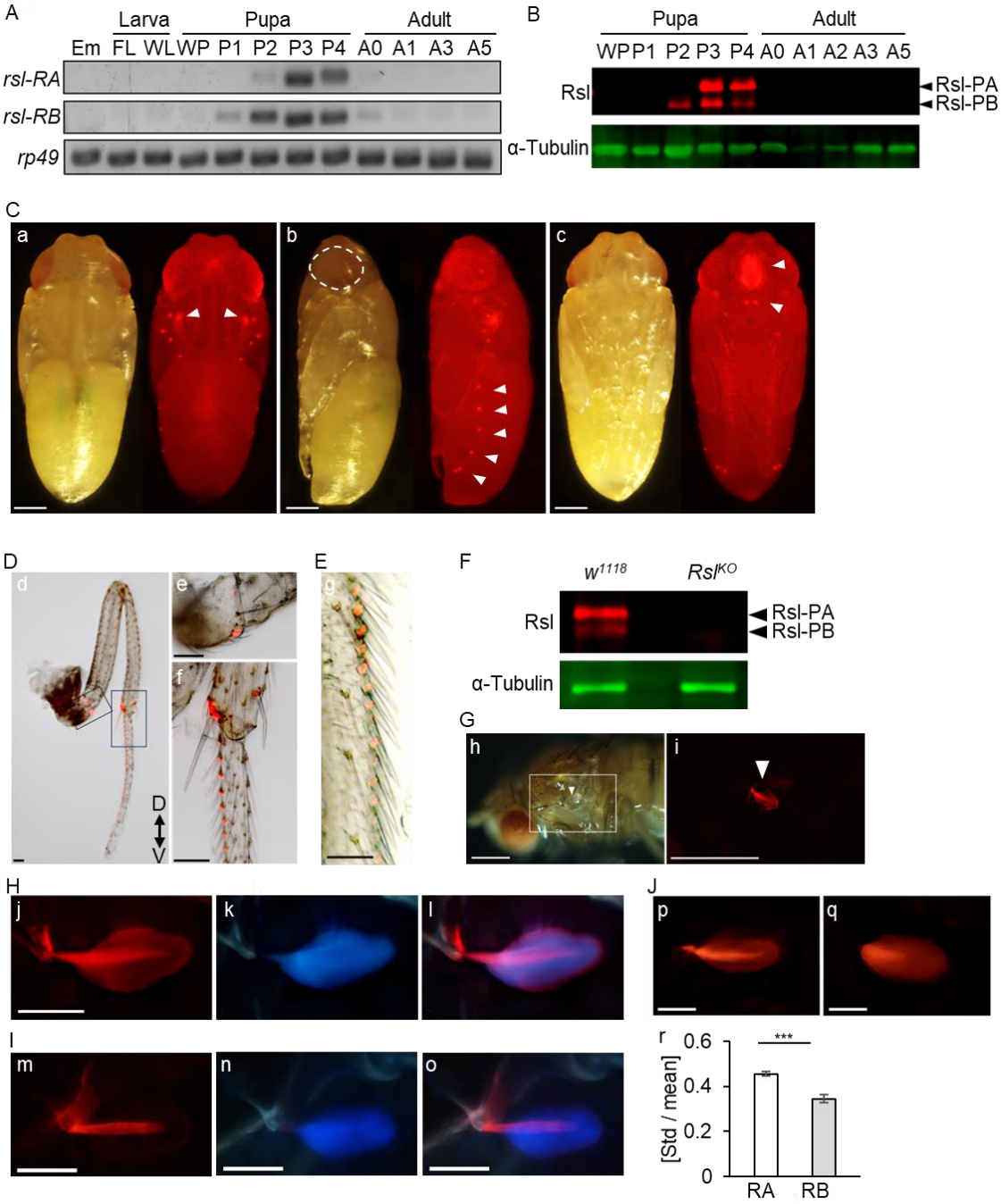
A
Larva
Pupa
Adult
Em FL WL WP P1 P2 P3 P4 A0 A1 A3 A5
rsl-RA
rsl-RB
rp49
B
Pupa
Adult
WP P1 P2 P3 P4 A0 A1 A2 A3 A5
Rsl
Rsl-PA
Rsl-PB
α-Tubulin
C
a
b
c
D
d
e
f
D
V
E
g
F
w1118
RslKO
Rsl
Rsl-PA
Rsl-PB
α-Tubulin
G
h
i
H
j
k
l
m
n
o
J
p
q
r
***
[Std / mean]
0.6
0.4
0.2
0
RA
RB

958 Figure 3

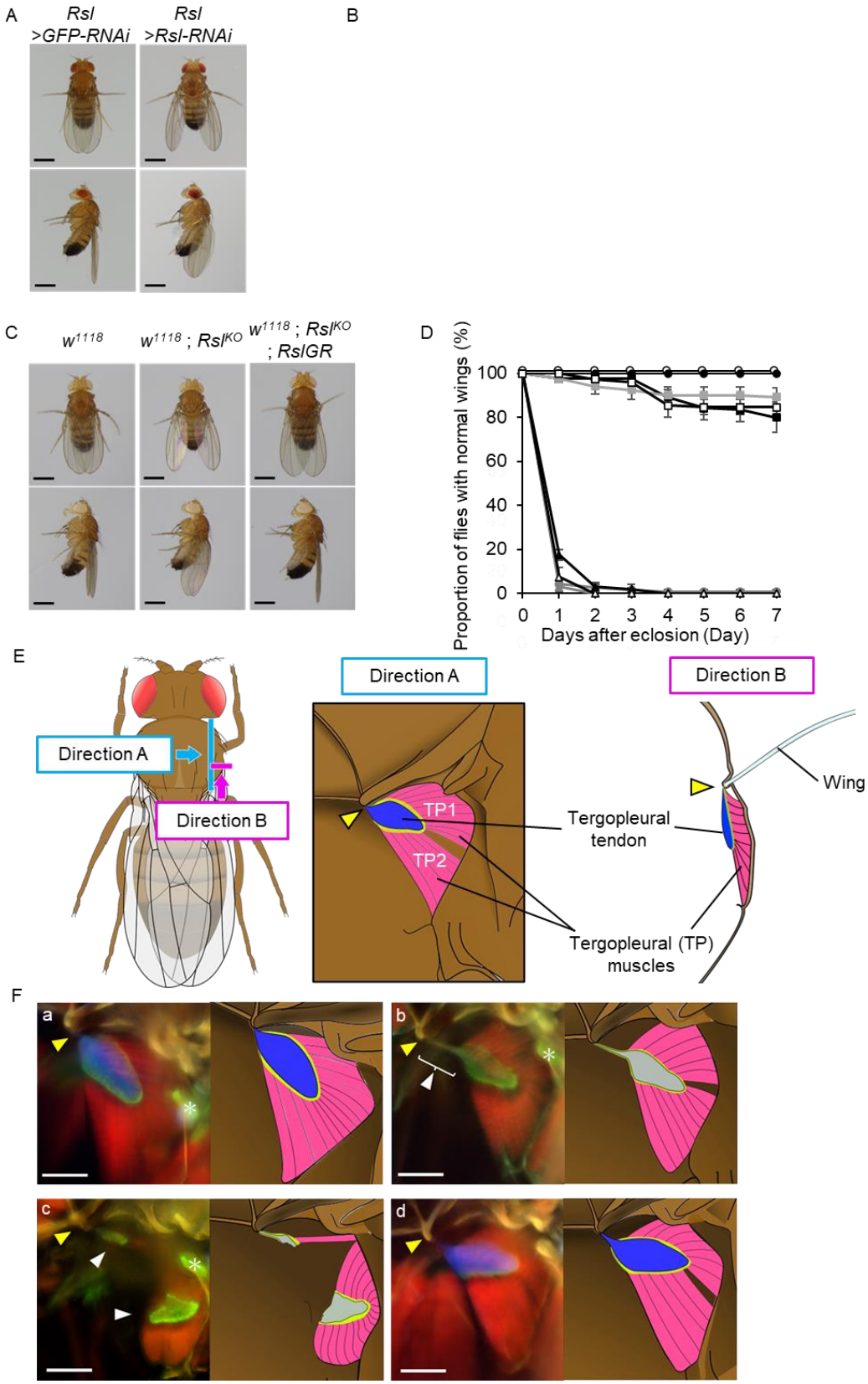

959

Figure 4-1

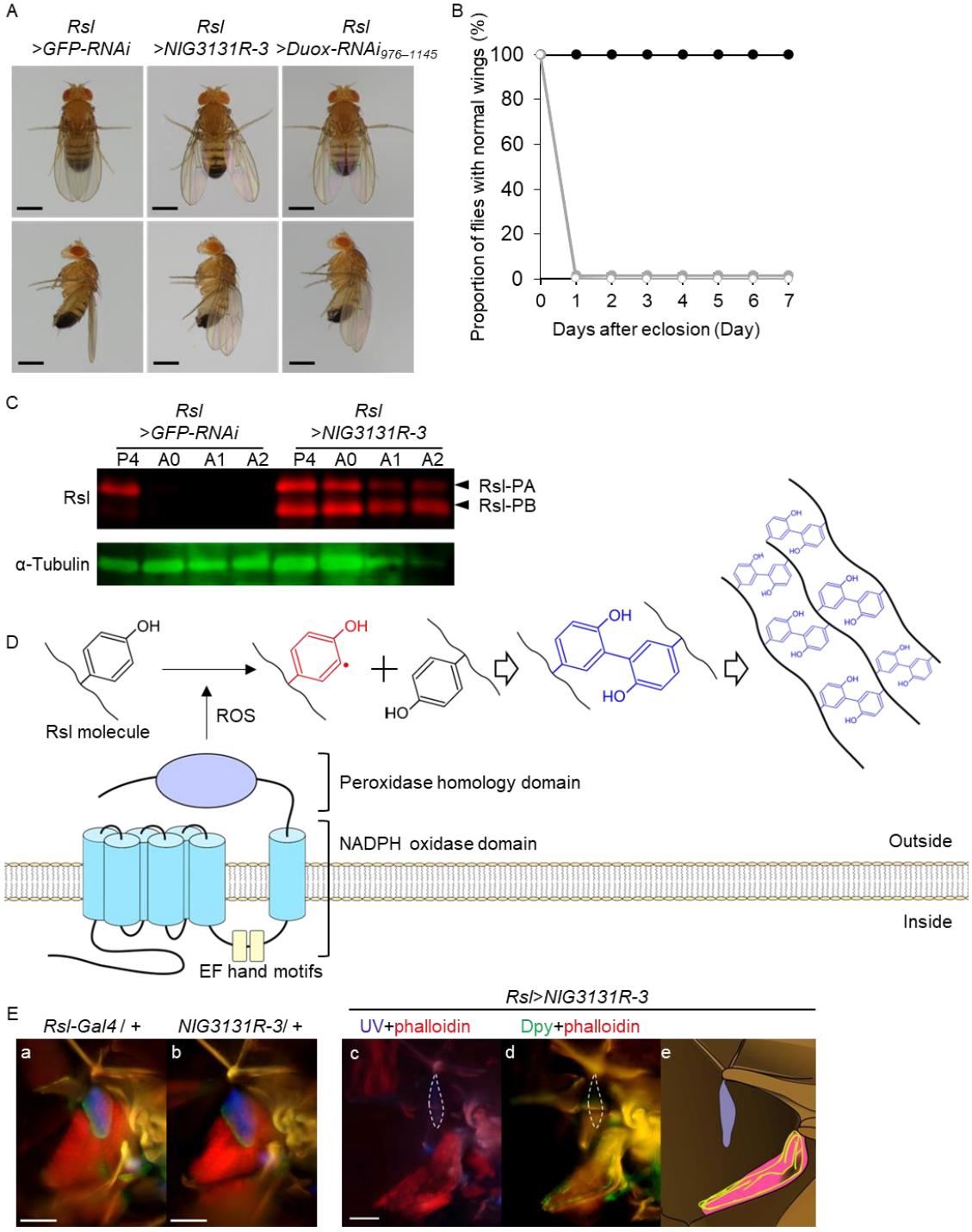
A
Rsl >GFP-RNAi
Rsl >NIG3131R-3
Rsl >Duox-RNAi976–1145
B
Proportion of flies with normal wings (%)
100
80
60
40
20
0
0 1 2 3 4 5 6 7
Days after eclosion (Day)
C
Rsl >GFP-RNAi
Rsl >NIG3131R-3
P4 A0 A1 A2 P4 A0 A1 A2
Rsl
Rsl-PA
Rsl-PB
α-Tubulin
D
OH
Rsl molecule
ROS
OH
HO
OH
HO
Peroxidase homology domain
NADPH oxidase domain
Outside
Inside
EF hand motifs
E
Rsl-Gal4 / +
NIG3131R-3/ +
Rsl>NIG3131R-3
UV+phalloidin
Dpy+phalloidin
a
b
c
d
e

Figure 4-2

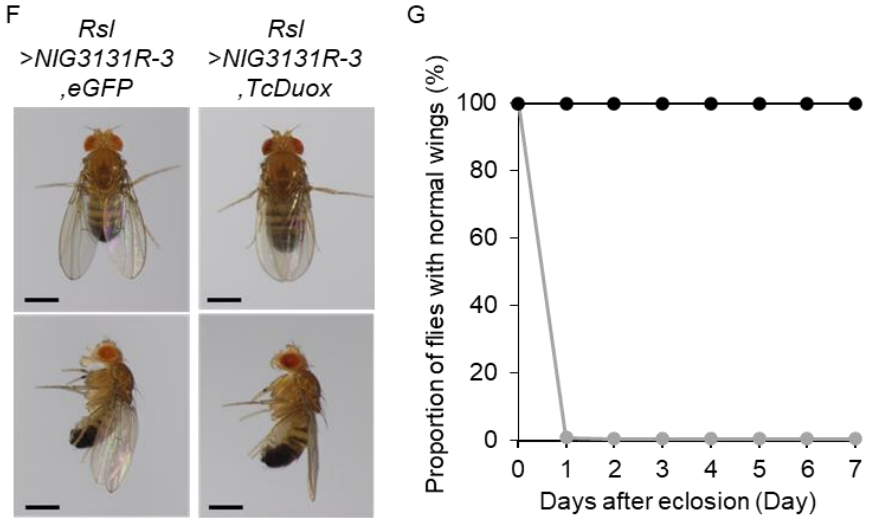
F
Rsl >NIG3131R-3 ,eGFP
Rsl >NIG3131R-3 ,TcDuox
G
Proportion of flies with normal wings (%)
100
80
60
40
20
0
0 1 2 3 4 5 6 7
Days after eclosion (Day)

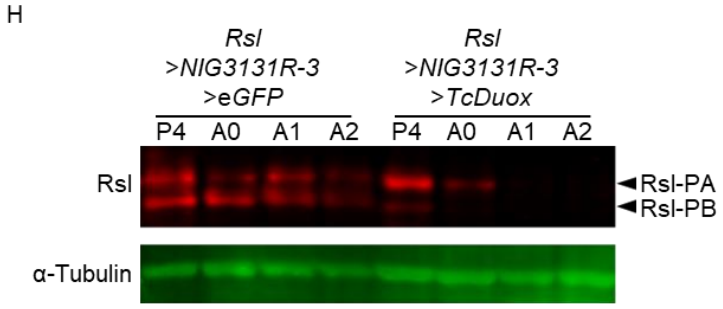
H
Rsl >NIG3131R-3 >eGFP
Rsl >NIG3131R-3 >TcDuox
P4 A0 A1 A2 P4 A0 A1 A2
Rsl
Rsl-PA
Rsl-PB
α-Tubulin

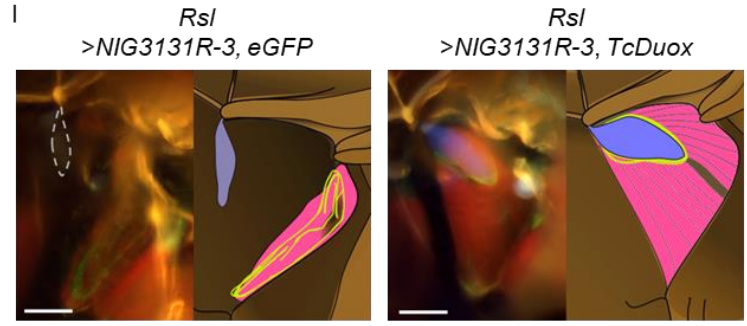
I
Rsl >NIG3131R-3, eGFP
Rsl >NIG3131R-3, TcDuox

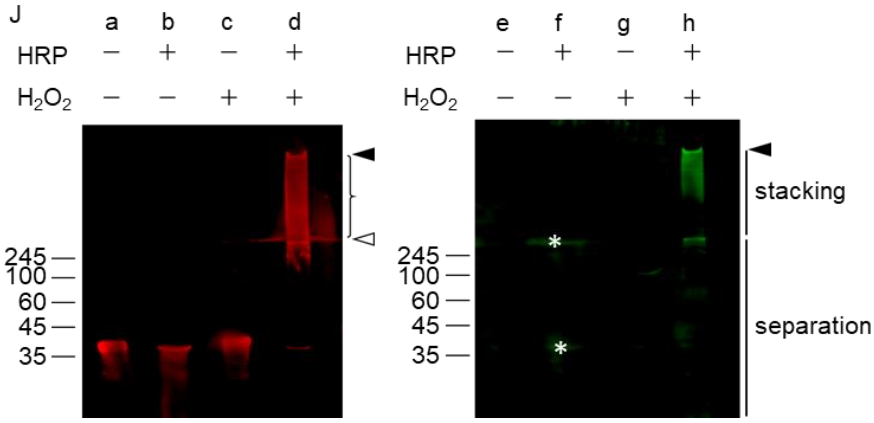
J
a b c d
HRP − + − +
H2O2 − − + +
245
100
60
45
35
e f g h
HRP − + − +
H2O2 − − + +
stacking
separation

964 Figure 5

965

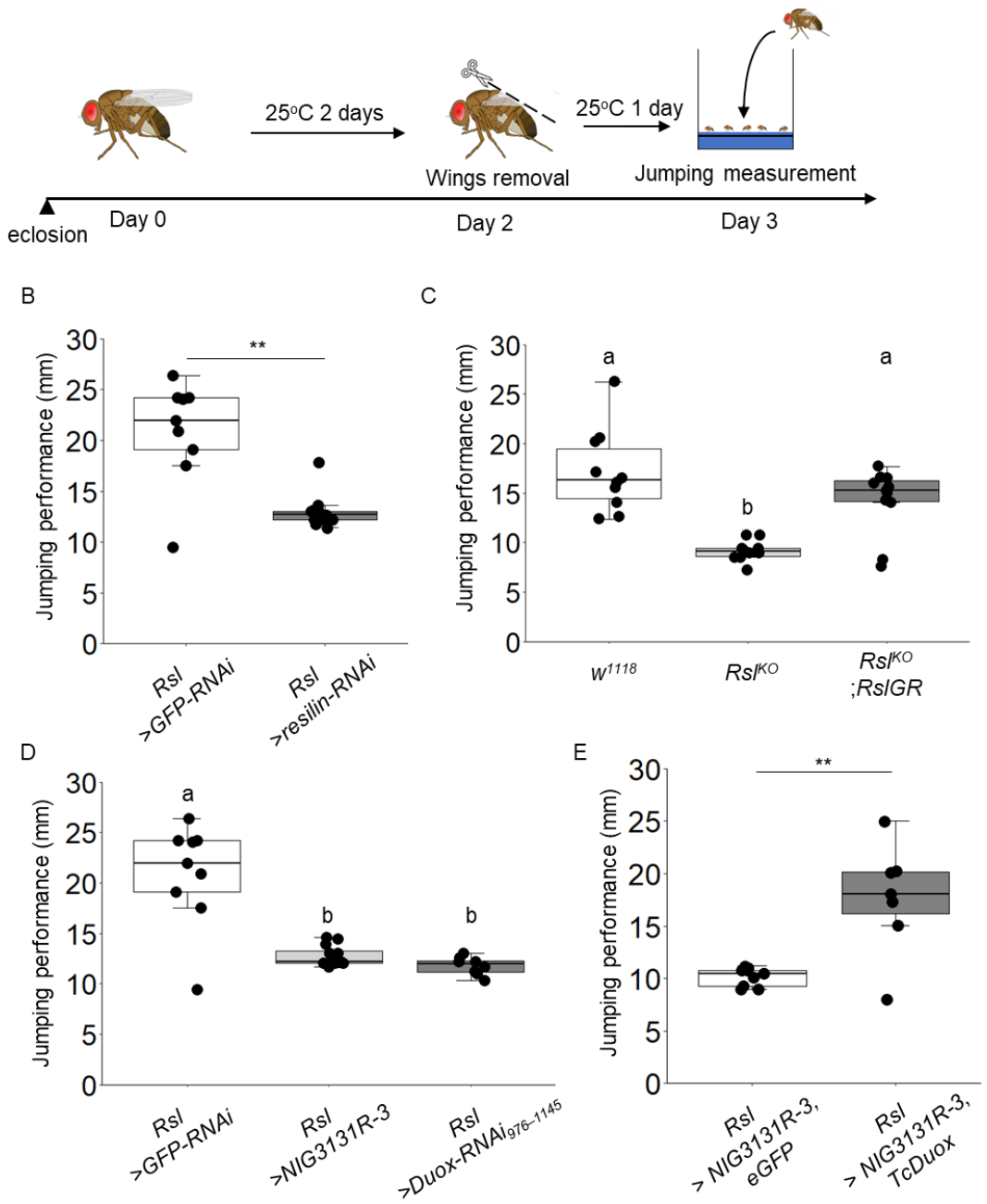

966

967

968